# Design Space Exploration and Performance Evaluation of a Multi-Chamber, Multi-Curvature Soft Actuator for Robotic Applications

#### Ansari Usama and Asokan Thondiyath

Department of Engineering Design, Indian Institute of Technology Madras, Chennai, 600 036, India

Keywords: Soft Actuator, Robotic Gripping, Parameter Identification, FEM.

Abstract:

Soft actuators are finding wide applications in robotics due to the compliance they offer in handling delicate objects. The design of soft actuators is challenging due to the fragile nature of the materials used and the difficulty of fabricating them. Also, soft actuators must be designed to achieve the desired bending performance that suits the application. This paper presents the design and analysis of a multi-chamber, multi-curvature soft actuator for robotic gripping applications. This design combines two different configurations to get the desired bending curvature of the actuator. Modeling of the actuator and analysis of the effect of various design parameters on the bending angle and the tip force are presented. Prototype fabrication and experimental results are also presented. The results confirm that it is possible to custom-design soft actuators to meet specific performance requirements through design synthesis.

#### 1 INTRODUCTION

Soft robots offer inherent compliance by using soft materials and novel structures to adapt to the surrounding environment, improving flexibility and adaptability. They take inspiration from nature, such as the octopus, starfish, and jellyfish. Soft robots aim to provide safe and compliant interaction with humans (Wu et al., 2019; Rogóż et al., 2016). Unlike traditional robots made from rigid links, joints, or inflexible components, soft robots are built using flexible and stretchable materials such as silicone rubbers, elastomers, and soft polymers, enabling them to achieve nearly infinite degrees of freedom, conform to various shapes and sizes, and manipulate fragile or irregular objects (Navas et al., 2021).

Traditional robotic grippers, made from hard materials like metal or plastic, are well suited for high-precision, repetitive tasks in structured environments due to their fast response, stability, and higher payload capacity. However, their limitations become evident in unstructured environments or tasks requiring delicate handling, such as grasping soft, fragile, or irregularly shaped objects (Zhang et al., 2019; Zhang et al., 2017). In contrast, soft grippers excel by utilizing compliant materials and bioinspired designs to offer safer, more adaptable

grasping solutions (Zaidi et al., 2021). The performance of soft grippers depends strongly on the design and bending behavior of soft actuators, which is the focus of this paper.

Various actuation methods for soft robots have been explored, including electroactive polymers, cable-driven systems, shape memory alloys, material jamming, magnetic actuation, and fluidics (pneumatic and hydraulic) (Su et al., 2022). Among these, pneumatic actuation is most widely adopted due to its simplicity, low cost, light weight, high force output, and ease of fabrication (Gariya et al., 2023).

The typical structure of a soft pneumatic actuator (SPA) consists of an extensible top layer with embedded air chambers and an inextensible bottom layer. When pressurized, the chambers expand and push against each other, causing the actuator to bend toward the inextensible side. To guide this deformation in a desired direction, the actuator is designed with differing material thicknesses between the chamber top wall and the inextensible bottom layer (Polygerinos et al., 2015).

SPAs can be either single-chamber or multichamber. Single-chamber actuators are easy to design and fabricate but tend to show significant radial expansion or ballooning effects under pressure, reducing precise control and efficiency (Gariya et al., 2023; Ariyano et al., 2019). Fiber reinforcement was introduced to overcome ballooning and enable directional bending by constraining deformation (Soft Robotics Toolkit, n.d.; Hu et al., 2018). Multichamber designs were introduced to overcome the difficulties with single-chamber actuators. A multicavity soft pneumatic actuator was developed in (Lei et al., 2022), and a theoretical model linking input pressure to bending deformation was proposed. Although the actuator demonstrated good flexibility, it was limited to a fixed single-curvature configuration. A structurally optimized multichamber soft actuator was proposed in (Hu et al., 2018), but it produces single-curvature bending. There were multiple approaches in the design of multi-chamber actuators through segmented control (Yang et al., 2020), multi-composite structures (Huang et al., 2021), and slow and fast pneumatic networks (sPN/fPN) (Mosadegh et al., 2014). These works demonstrate continued progress in improving actuation performance and structural optimization, yet most remain limited to single-curvature, singleconfiguration outputs. Such actuators are unsuitable for many robotic grasping applications because they struggle to conform to irregular shapes or delicate objects, point contact at the actuator tip, have limited surface conformability, and the contact force generated is less uniform (Tang et al., 2022). (Song et al. 2021) achieved multi-curvature deformation by dividing the multi-chamber actuator into several chamber groups and actuating those selectively using independent pressure channels. This enabled programmable deformation patterns and improved dexterity but required complex multi-channel pneumatic control, increasing system-level complexity.

Building on our earlier work (Ansari et al., 2025), this paper proposes a multi-chamber, multi-curvature bending profile soft actuator using a multi-curvature design and a single pneumatic channel. The actuator also integrates an adhesion mechanism to improve further grasping stability and adaptability. Performance metrics, including taper optimization, contact uniformity, and object compatibility, are evaluated through numerical simulations and parametric studies, demonstrating advantages of this approach over conventional single curvature designs.

The remainder of the paper is organised as follows: Section 2 provides Methodology, Section 3 explains Parametric Study, Section 4 provides Biomimicry in Soft Actuator Design with Suckers, Section 5 provides Simulation Studies, Section 6 includes Prototyping and Testing, Section 7 Actuator

Testing for Grasping, and Section 8 provides Conclusion and future work, followed by References.

#### 2 METHODOLOGY

The design of the soft actuator is achieved by combining design configurations of air chambers, as shown in Figure 1. The series arrangement of Configuration B–C–A is inspired by the work of (Ansari et al. 2025), while Configurations A and B are based on (Mosadegh et al. 2014), and Configuration C draws inspiration from (Yang et al. 2020).



Figure 1: Sectional view of SPA for Configuration B, C, A.

Referring to Figure 1, Configuration A has no gap between chambers, which leads to high stiffness and limited bending. Configuration B has gaps present but chambers are attached to the bottom plate, which slows bending. In contrast, in Configuration C, the chambers are detached from the bottom plate, leading to fast, less restricted bending.

Therefore, the proposed design combines Configurations B and C, with seven chambers for Configuration B and five for Configuration C, as shown in Figure 2. Figure 3 shows the cross-sectional view of the actuator. Parameter identification and performance analysis were done to identify the best design parameters for the proposed design configuration.

This process was done in two steps: first, optimizing the taper angle by inclining the four lateral faces of the rectangular cross-section inward, inspired by tapering seen in octopus arms and elephant trunks, which improves bending (Calisti et al. 2011), and second, performing a parametric analysis of geometric dimensions such as chamber gap, wall thickness, and other structural parameters.

# 2.1 Design Variants for Taper Optimization

A systematic design study was performed to identify the best taper angle for the multi-chamber, multicurvature soft actuator. Several design variants were defined by varying the inclination of the lateral faces of the rectangular cross-section of the actuator tapering on actuator performance, inspired by octopus arms and elephant trunks. Figures 4(a) and (b) show the taper angle variations proposed in this study. Table 1 summarizes the different design variants, their descriptions, and the sets considered to support the selection of the optimal design variant for further parametric analysis.

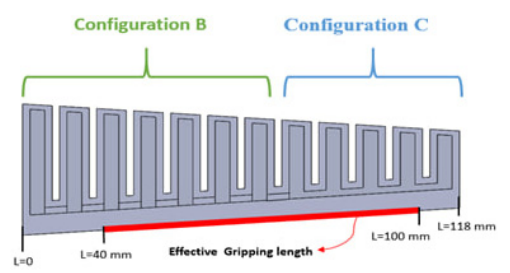


Figure 2(A): Sectional View with Configuration B & C.

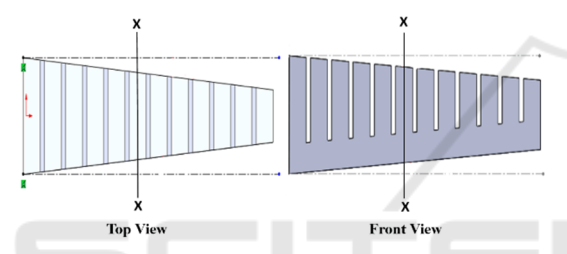


Figure 2(B): CAD Model of SPA with Configuration B&C.

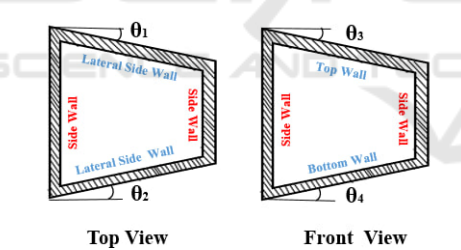


Figure 3: Sectional view of SPA at Section X-X.

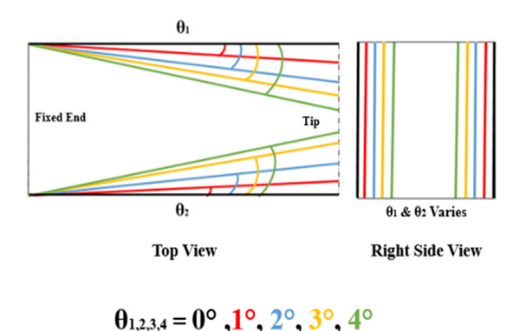


Figure 4: (A) Taper Angle Variation for SPA (Top View).

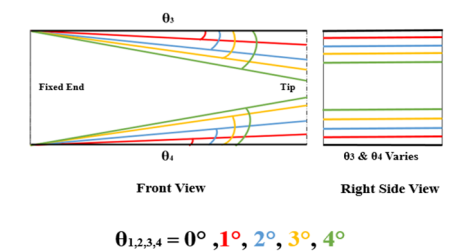


Figure 4: (B) Taper Angle Variation for SPA (Front View).

## 2.1.1 Design Variant Simulation Study and Ranking Methodology

A systematic simulation study was carried out to evaluate the bending performance. Each design variant was modelled with specific combinations of taper angle. 64 variants were analyzed and labelled as different "sets" (for example, Set B, Set C, Set D), where each set denotes a taper condition for each actuator variant, a finite element simulation was conducted in Abaqus/CAE to evaluate the bending deformation under applied internal pressure, where the actuator was modelled using a hyperelastic material model (Yeoh model) to capture its nonlinear elastic behaviour, and the analysis was performed using a nonlinear static step. Boundary conditions were applied by fixing the base of the actuator, while pressure loading was applied uniformly to the inner chamber surfaces. Further details on the geometry, meshing, material properties, and loading are provided in Section 5.

The key parameters recorded along the effective gripping length (from 40 mm to 100 mm) were:

- Bending angle  $(\theta)$ : the angular change between the base and tip,
- Slope of the actuator (s): the average angular gradient along the curved body,
- Tip deflection (d): the vertical displacement of the actuator tip from its original position, as shown in Figure 5.

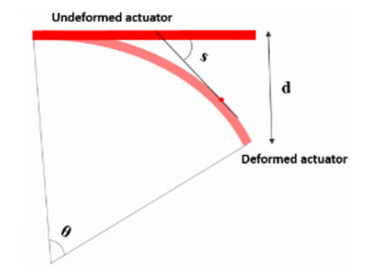


Figure 5: Illustration of actuator deformation parameters.

Design Variant	Description	Set (At Section X-X)
1	All four faces varied from 1°- 4° taper, forming sets A – D based on different taper assignments. 4 combinations formed. (1 variation per set).	1 2 3 4 D 4 1 2 B 2 3 C 3 4 D 4
2	One face fixed at 0°, other three faces varied from 1°-4° taper, forming sets A-D. 16 combinations formed (4 sets × 4 taper variations in each set).	v A v 0 B v v C v V D 0
3	Two faces fixed at 0°, other two faces varied from 1°-4° taper, forming sets A-F. 24 combinations formed (6 sets × 4 taper variations in each set).	0 A V 0 B 0 V C V 0 D V V E 0 V F 0
4	Three faces fixed at 0°, one face varied from 1°-4° taper, forming sets A–D. 16 combinations formed (4 sets × 4 taper variations in each set).	0 A 0 0 B V 0 C 0 V D 0
5	All four faces tapered differently, with angles of 1°, 2°, 3°, and 4° assigned in permutations to form sets A–D. 16 combinations formed (4 sets × 4 permutations).	1 A 3 4 B 2 3 C 1 2 D 4
V	denotes a face with taper angle varied from 1° to 4° in the study	0 denotes a face with zero angle.

Table 1: Design variants considered for taper angle optimization in multi-chamber soft actuator.

A multi-criteria ranking metric was developed to objectively compare the variants, based on two criteria: average performance and uniformity of bending.

The scoring was calculated as follows:

Final Score = 0.5×Average Weighted Score + 0.5× (1–Average Normalized Variance) where, the weighted score combines normalized values of bending angle (0.4 weight), slope (0.3 weight), and deflection (0.3 weight), this weight is assigned based on the relative importance in grasping tasks.

Weighted Score= $0.4\times$  (Normalized Bending) + $0.3\times$  (Normalized Slope) +  $0.3\times$ (Normalized Deflection)

The normalization for bending, slope, and deflection metrics was computed using min-max normalization, i.e.

Normalized Value = 
$$\frac{\text{Value} - \min(\text{Value})}{\max(\text{Value}) - \min(\text{Value})}$$

where the min and max were computed across all configurations over the effective gripping range (40 mm to 100 mm).

The Average Weighted Score is computed by averaging the weighted scores across the seven evaluation points in the gripping zone. The Average Normalized Variance quantifies how consistently the actuator performs along its length, by calculating the variance of slope values normalized over the same evaluation region.

Based on the final scores as in Table 2, Variant 4D with a 4° taper had the highest rank. However, its asymmetric left-sided taper produced a diagonal or inclined bending profile that was less suitable for gripping. Therefore, Variant 3C with a 2° taper was chosen, as both the side faces are tapered equally for further experimental validation. This variant showed a high bending angle, consistent slope distribution, and a balanced deflection profile, making it better suited for soft gripping applications where predictable, symmetric bending is critical.

# 2.1.2 Taper Angle for Selected Design Variants (3C2)

In this study, the actuator cross-section was rectangular, and the tapering of the side faces was varied to evaluate its effect on bending performance Variants were categorized based on how many faces were tapered and at what angle.

Design Variant	Set	Taper Angle	Avg Weighted Score	Avg Normalized Slope Variance	Final Score	Rank
4	D	4°	0.648	0.269	0.6729	1
3	С	2°	0.637	0.264	0.6667	2
2	В	1°	0.632	0.266	0.6626	3
3	С	1°	0.632	0.266	0.6626	3
3	F	2°	0.624	0.275	0.6543	5

Table 2: Top 5 Ranked Design Variants Based on Weighted Performance Score and Normalized Slope Variance.

- Design Variant 3: Two faces were fixed at 0° (no taper), while the other two were tapered at equal angles ranging from 1° to 4°.
- Set C of Variant 3 (3C): Corresponds to a specific face arrangement where the top and bottom faces are fixed at 0°, and the left and right faces are tapered.
- 3C2: In this configuration, the left and right faces were tapered inward at 2°, while the top and bottom faces remained at 0.
- This design variant helps bending of actuator inwards, as the tapered sides make it easier for the walls to bend in that direction.
- Figure 6 illustrates the rectangular crosssection from right-side and top views, indicating the fixed and tapered faces ( $\theta_1 = 0^\circ$ ,  $\theta_2 = 0^\circ$ ,  $\theta_3 = 2^\circ$ ,  $\theta_4 = 2^\circ$ ).

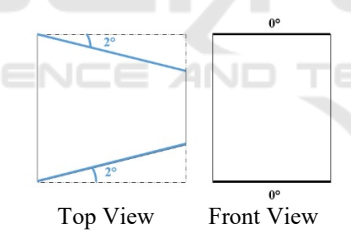


Figure 6: Sectional Diagram for Design Variant 3C2.

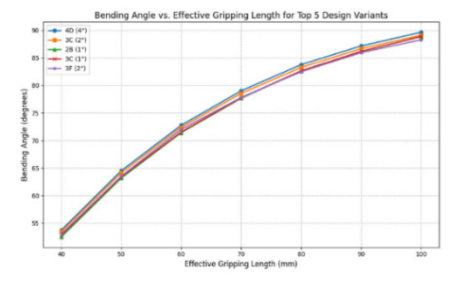


Figure 7: Bending Behaviour for top design variant.

The selected Design variant 3C2 sectional view, CAD model and simulation is shown in Figure 8

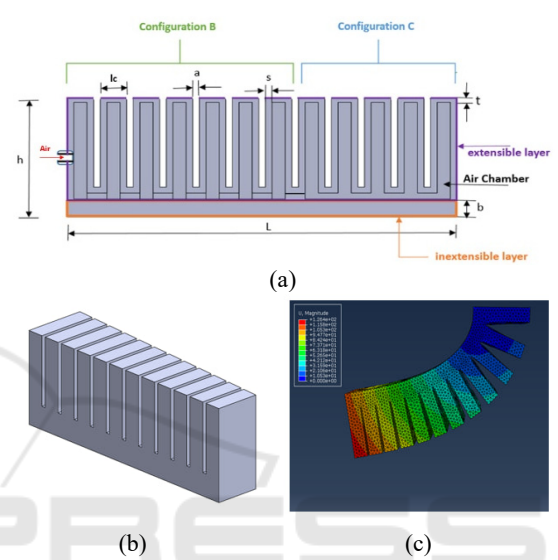


Figure 8: (a) Actuator Sectional View and (b) CAD Model for 3C-2 degree (c) Simulation.

### 3 PARAMETRIC STUDY (3C2)

A parametric study systematically investigates how changing individual geometric parameters affects the actuator's bending behaviour and overall performance.

The objectives of the study are:

- 1. **Understand the Sensitivity**: Know which parameters significantly influence the performance (e.g., bending angle, force, and displacement).
- 2. **Optimize the Design**: Identify the best parameters for desired performance (e.g., maximum bending angle).
- 3. **Improve Efficiency**: Reduce material cost, air consumption, and increase reliability.
- 4. **Design Guidelines:** Propose guidelines for future designs or prototypes.

To assess performance changes, two metrics were used: Sensitivity (°/kPa), which measures how much the bending angle changes per unit pressure (higher values mean faster bending but harder control), and

R<sup>2</sup>, which measures how well pressure predicts bending (values near 1 mean more consistent and reliable control)

The parameters examined include: chamber gap, sidewall thickness, gap shape, actuator width, top wall thickness, and bottom wall thickness. The results and analysis for each parameter are presented in the following subsections.

#### 1. Chamber Gap

The chamber gap, i.e, spacing between adjacent chambers, affects bending angle, sensitivity, and control predictability. FEA results for 1 mm, 2 mm, and 3 mm gaps (Figure 9) show that the bending angle is inversely proportional to gap size. A 1 mm gap yields the highest sensitivity (1.62°/kPa) due to strong inter-chamber interaction, but lower predictability (R² = 0.973) and complex fabrication. A 3 mm gap minimizes interaction, giving the lowest sensitivity (1.22°/kPa) but slightly better predictability (R² = 0.983). The 2 mm gap offers a balance with moderate sensitivity (1.45°/kPa), highest predictability (R² = 0.987), and ease of manufacturing, thus selected as optimal.

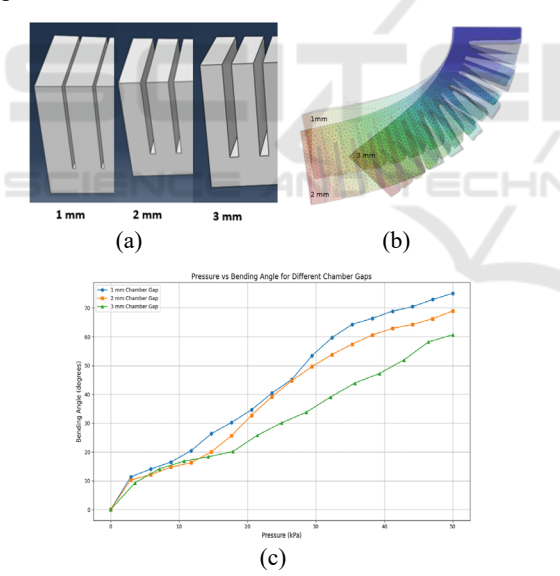


Figure 9: (a) Chamber Gap (b) FEA Simulation (c) Pressure and Bending Angle variation.

#### 2. Side Wall Thickness

The side wall, i.e, the outer enclosure of each air chamber, affects actuator flexibility, pressure resistance, and deformation. FEA simulations for thicknesses of 1 mm, 2 mm, and 3 mm (Figure 10) show bending angle is inversely proportional to wall thickness: thicker walls enhance pressure resistance

but reduce flexibility. At 1 mm, the actuator achieved the highest bending sensitivity (1.718 °/kPa) but slightly reduced predictability ( $R^2=0.997$ ) and a higher risk of ballooning. At 3 mm, stiffness limited bending, yielding the lowest sensitivity (1.052 °/kPa) and predictability ( $R^2=0.963$ ). The 2 mm wall provided an optimal balance with moderate sensitivity (1.412 °/kPa), good predictability ( $R^2=0.973$ ), and adequate structural stability, making it the preferred choice.

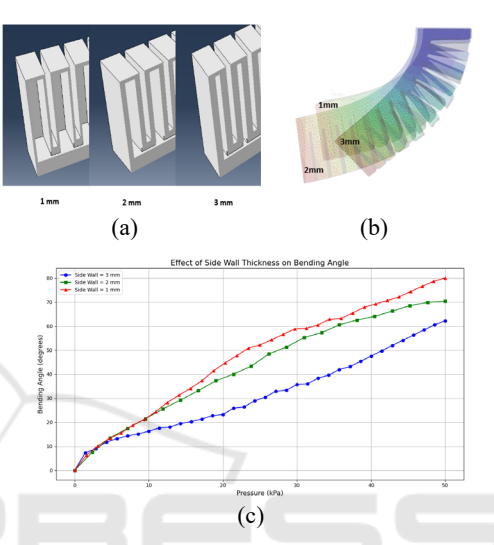


Figure 10: (a) Side Wall (b) FEA Simulation (c) Pressure and Bending Angle variation.

#### 3. Gap Shape

The gap shape, i.e the geometric profile of the space between adjacent chambers influences deformation and stress distribution. Four geometries were studied: rectangular (conventional), trapezoidal, U-shaped, and V-shaped (Figure 11). The rectangular gap delivered the highest bending sensitivity (1.41°/kPa) and strong predictability ( $R^2 = 0.973$ ), ensuring consistent deformation and mechanical efficiency. The U-shape offered moderate sensitivity (1.08°/kPa,  $R^2 = 0.967$ ) with balanced stress distribution and ease of fabrication. The V-shape showed slightly lower sensitivity (1.05 $^{\circ}$ /kPa, R<sup>2</sup> = 0.963) and risk of localized stress. The trapezoidal shape minimized stress concentration but had the lowest sensitivity (1.03°/kPa,  $R^2 = 0.961$ ) and slower actuation. The rectangular gap was selected for the final design due to its superior performance and manufacturing simplicity.

#### 4. Width of Actuator (Tapered Profile)

The actuator width, i.e, total lateral dimension at the base of chambers with a 2° taper based on 3C2 optimization, affects bending capability, pressure

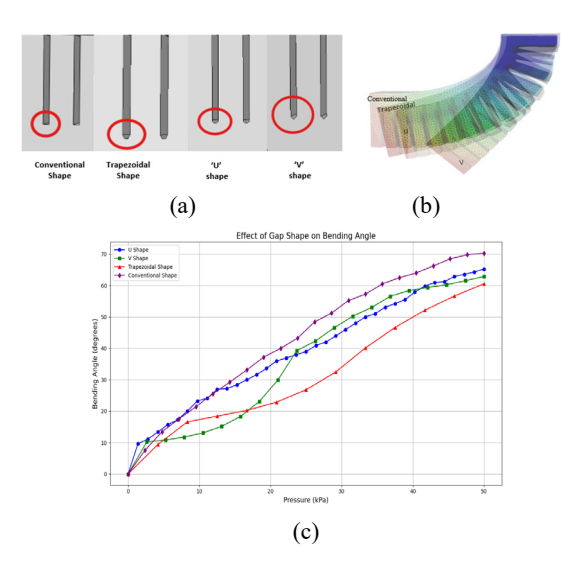


Figure 11: (a) Gap Shape (b) FEA Simulation (c) Pressure and Bending Angle variation.

response, and stability. Three widths: 26 mm, 30 mm, and 34 mm, were tested (Figure 12). The 34 mm width showed the highest bending sensitivity (1.41°/kPa, R² = 0.973) but increased material use and reduced stiffness. The 26 mm width offered higher stiffness and faster response but slightly lower sensitivity (1.05°/kPa, R² = 0.963). The 30 mm width achieved balanced performance (1.08°/kPa, R² = 0.967), combining substantial bending, stability, and ease of manufacturing. It was selected as optimal, avoiding the over-deformation of wider profiles while maintaining high controllability.

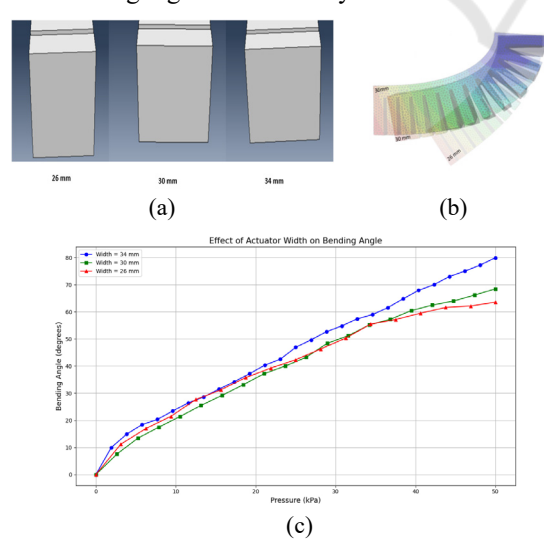


Figure 12: (a) Width at fixed end (b) FEA Simulation (c) Pressure and Bending Angle variation.

#### 5. Top Wall Thickness

Top wall thickness i.e material layer sealing each chamber from above, inversely proportional to bending angle, influences pressure containment, bending range, and deformation uniformity. FEA tests on 1 mm, 1.5 mm, and 2 mm thicknesses (Figure 13) showed that 1 mm yielded the highest sensitivity (1.52°/kPa, R² = 0.971) but reduced pressure resistance and increased ballooning risk. The 2 mm wall was stiffest (1.05°/kPa, R² = 0.963), limiting bending but improving high-pressure durability. The 1.5 mm thickness provided balanced performance (1.26°/kPa, R² = 0.969), offering substantial bending with improved stability, and was selected as optimal.

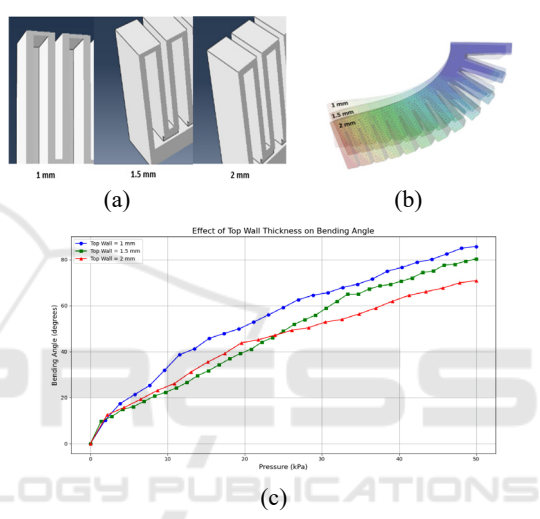


Figure 13: (a) Top wall (b) FEA Simulation (c) Pressure and Bending Angle variation.

#### 6. Bottom Wall Thickness

Bottom wall thickness defines the actuator's ability to resist vertical deformation under internal pressure, influencing stability and bending performance. FEA tests on 5 mm, 6 mm, and 7 mm thicknesses show an inverse relation with bending angle, as in Figure 14. The 5 mm wall had the highest sensitivity (1.48 °/kPa,  $R^2 = 0.972$ ) but higher bulging risk; the 7 mm wall was most rigid (1.06 °/kPa,  $R^2 = 0.965$ ) but limited bending. The 6 mm wall offered balanced sensitivity (1.25 °/kPa,  $R^2 = 0.970$ ), good durability, and manufacturability, making it optimal.

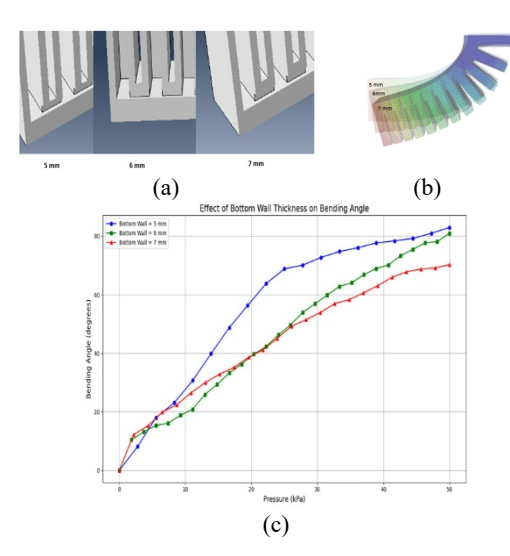


Figure 14: (a) Bottom wall (b) FEA Simulation (c) Pressure and Bending Angle variation.

### 4 BIO-MIMICRY OF MODIFIED SOFT ACTUATOR DESIGN WITH SUCKERS

Biomimicry draws inspiration from nature's forms, processes, and systems to inspire engineering solutions (Benyus 1997). The modified soft actuator here takes inspiration from the octopus tentacle, which is a flexible, tapered, boneless structure with rows of suckers decreasing in size toward the tip. The suction force generated by a suction cup is given by:  $F = AP \times A$ 

where  $\Delta P$  is the pressure difference (assumed vacuum pressure: -50 kPa, atmospheric pressure: 101.3 kPa), and  $A=\pi r^2$  is the effective area. Five suckers were considered with radii from 5 mm to 9 mm.

A simulation study in Figure 15 shows that adding more suckers increases total suction force by enlarging the contact area, but too many suckers reduce the actuator's bending angle due to increased surface stiffness. To balance adhesion with flexible bending, three suckers were selected, placed at 40 mm, 70 mm, and 100 mm along the actuator, with diameters of 20 mm, 18 mm, and 16 mm, respectively. This configuration optimizes surface contact, sealing, and bending for effective gripping of spherical or irregular objects as shown in Figure 16.

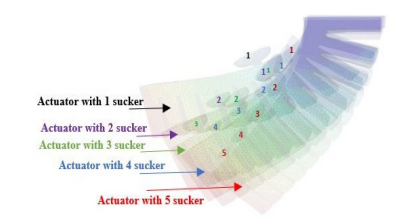


Figure 15: Simulation for number of suckers.

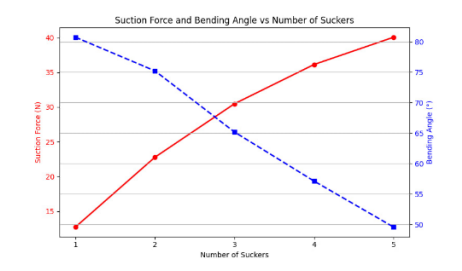


Figure 16: Suction Force vs Bending Angle vs Number of Suckers.

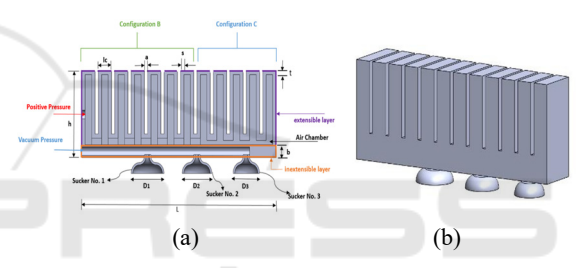


Figure 17: (a) Actuator Sectional View (b) CAD Model for 3C-2 degree with Sucker.

Table 3: Parameters of SPA.

Parameters	Value (mm)
Side wall thickness (s)	2
Top wall thickness (t)	1.5
Chamber gap (a)	2
Bottom layer (b)	6
Width at base	30
Sucker Diameter (D1)	20
Sucker Diameter (D2)	18
Sucker Diameter (D3)	16

#### 5 SIMULATION STUDIES

The soft actuator was simulated and analysed using the standard explicit model in ABAQUS/CAE 6.14 (Dassault Systems, 2021) to study the bending angle under different pressure conditions. The material parameters used for 3D printing 50A resin was used in the simulation. The material coefficients  $C_{10} = 0.25$  MPa,  $C_{20} = -0.05$  MPa,  $C_{30} = 0.005$  MPa (Sun et al., 2019), were used for Yeoh hyper elastic

mathematical model to characterize the nonlinear stress-strain behaviour of the soft actuator.

Since the actuator undergoes large deformations with nonlinear effects in simulation, Nlgeom was activated 'ON'. The selected mesh type was 3D stress, 10-node quadratic tetrahedral hybrid elements (C3D10H).

A mesh convergence study was performed with varying global mesh sizes (ranging from 1.5 mm to 4.0 mm).

A mesh size of 2.5 mm was selected as it offered a good balance between simulation accuracy and computational efficiency, with negligible variation observed in deformation behavior upon further refinement as shown in Figure 18.

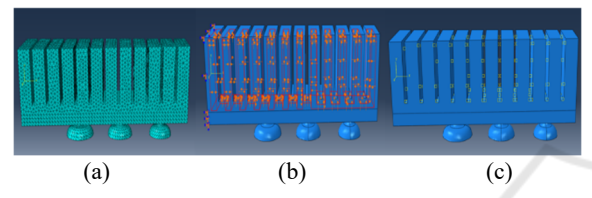


Figure 18: (a) Meshing (b) Gravity Load, Internal Pressure, BC (c) Self Contact Interaction.

#### 6 PROTOTYPING AND TESTING

The soft actuator was fabricated using SLA (Stereo lithography) 3D printing on a Formlabs Form 3L printer with Elastic 50A resin, a flexible material suitable for pneumatic actuation. The process began with cleaning the build plate, loading the resin tank and cartridges, and preparing the print file using PreForm software for optimal orientation and support. The final prototype is shown in Figure 19.

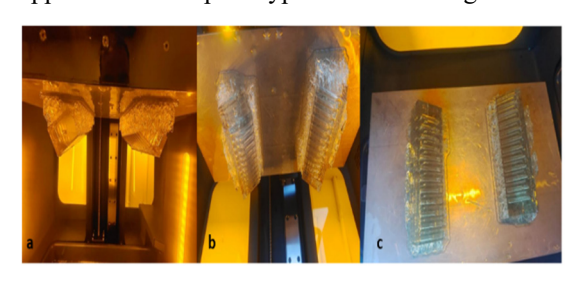




Figure 19: (a-c) 3D Printing Steps, (d) Final prototype.

The experimental setup, along with a schematic diagram of the experimental setup, is shown in Figure 20.

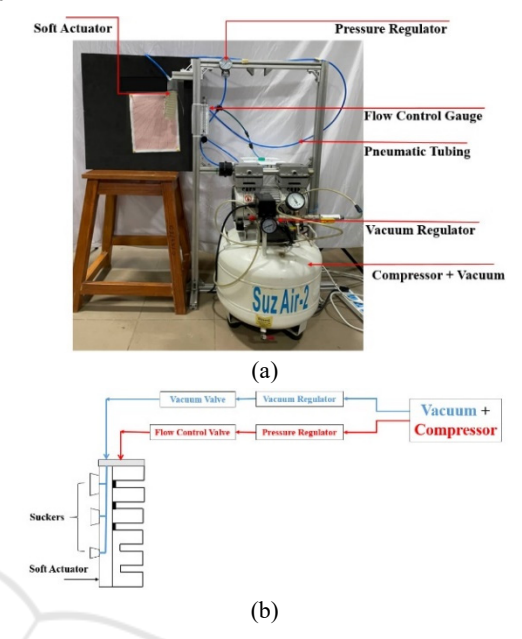


Figure 20: (a) Experimental Setup (b) Schematic Diagram for SPA.

### 6.1 Bending Angle Measurement

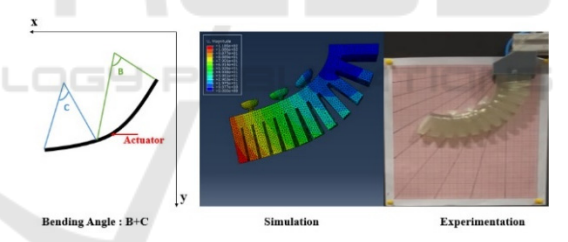


Figure 21: Bending angle of the actuator.

Figure 21 explains the methodology adopted for the bending angle measurement of the multi-chamber actuator. Figure 22 shows a comparison of the bending angle for simulation and experiment.

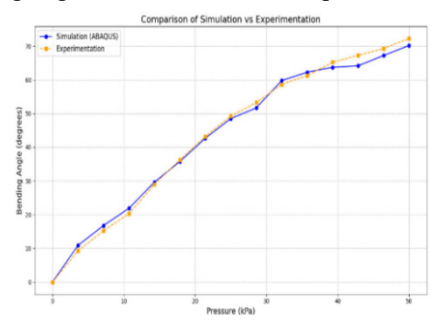


Figure 22: Bending angle wrt Pressure: Comparison of Simulation and Experimental results.

### 6.2 Error Analysis

To validate accuracy, an error plot of absolute bending angle deviation between simulation and experiments shows differences within 2° across the pressure range, confirming strong agreement as shown in Figure 23. Minor discrepancies may arise from material nonlinearity, fabrication tolerances, or experimental variability.

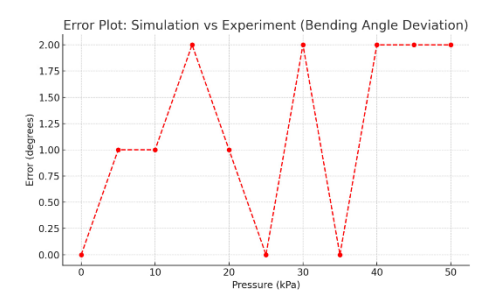


Figure 23: Bending Error Analysis.

# 6.3 Multi-Curvature Bending Shape and Tip Trajectory Analysis

Two deformation analyses were conducted for the multi-chamber, multi-curvature soft actuator.

Bending profiles were plotted at various pressures by tracking midline points, revealing non-uniform, multi-curvature bending shown in Figure 24. This behavior enhances dexterity and spatial adaptability in soft robotic tasks.

Tip trajectories were obtained from experimental video tracking and Abaqus/CAE simulations by recording X–Y displacements of the actuator tip relative to the base. The curves show nonlinear tip motion with pressure, reflecting multi-configuration deformation shown in Figure 25.

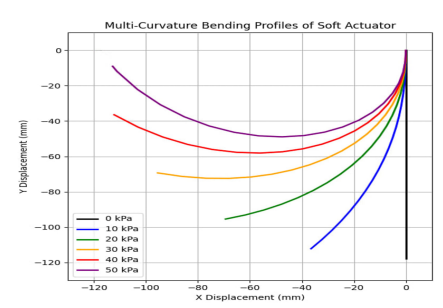


Figure 24: Bending Curve Profiles.

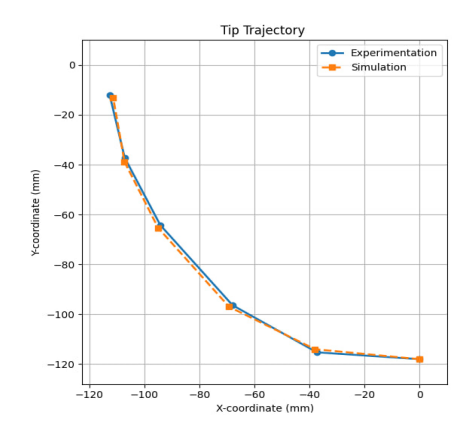


Figure 25: Tip Trajectory.

### 6.4 Curvature Adaptability Index (CAI)

The CAI measures how effectively an actuator changes curvature with pressure, which is critical for adaptable grasping and shape conformity. For the 118 mm multi-chamber, multi-curvature actuator, the CAI between 10 kPa and 50 kPa is 0.1886 rad·m<sup>-1</sup>·kPa<sup>-1</sup>, equivalent to a bending sensitivity of 1.275°/kPa, indicating high curvature responsiveness and precise deformation control.

#### 7 ACTUATOR GRASPING TEST

The Bending and Gripping capability of the Single actuator was tested as discussed below.

(a) A small rubber ball was chosen to test the actuator's ability to handle compact and delicate items. The actuator successfully demonstrated its capability to conform to and grip this ball, as illustrated in Figure 26.

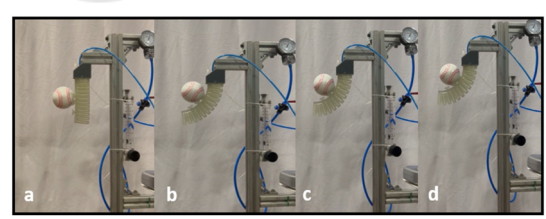


Figure 26: Demonstration of grasping of a rubber ball.

(b) A smooth, soft plastic ball was used to test the actuator's ability to adapt to bigger, lightweight spherical objects. The actuator reliably grasped and held this object, as illustrated in Figure 27.

Reference	Туре	Curvature Profile	Key Features
Gariya et al., 2023	Single chamber	Single	Ballooning, limited control
Song et al., 2021	Multi-chamber with grouped	Multi	Programmable deformation, improved dexterity, Multi- channel, Complex pneumatic system
Ansari et al., 2025	Multi-chamber	Multi	Low output force, no adhesion
Ansari et al., 2025 (Proposed)	Multi-chamber	Multi	Improved curvature range, integrated adhesion i.e suction for better grasps adaptability

Table 4: Comparison of Proposed Actuator with Existing Designs from Literature.

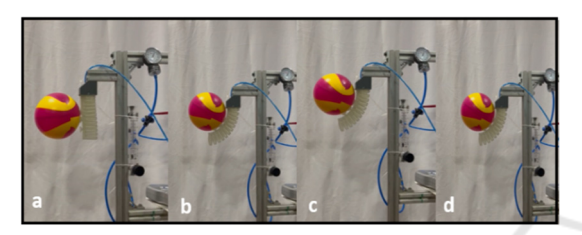


Figure 27: Demonstration of grasping a plastic ball.

#### 8 COMPARATIVE ANALYSIS

The proposed multi-chamber, multi-curvature soft pneumatic actuator was compared with recent literature and a previous in-house prototype (Ansari et al., 2025), as summarized in Table 4. It shows that the proposed actuator is superior to the available soft actuators.

# 9 CONCLUSIONS AND FUTURE SCOPE

This work presented a bioinspired multi-chamber, multi-curvature soft pneumatic actuator with integrated suction cups, designed for variable bending curvature and adaptive grasping. Using Yeoh hyperelastic model and FEA, the design space was explored through parametric studies on chamber gap, wall thickness, and taper angle. Tip trajectory and Bending Curve profile confirms the multi-curvature effects. The actuator achieved a Curvature Adaptability Index (CAI) of 0.1886 rad·m<sup>-1</sup>·kPa<sup>-1</sup> and bending sensitivity of 1.275°/kPa for a 118 mm length, outperforming conventional single-curvature designs in curvature adaptability and tip deflection.

Future work will address these through asymmetry metrics for design evaluation, inverse optimization for predictive modeling, multi-finger gripper integration, exotic chamber geometries, embedded sensing, and closed-loop control for precision grasping, aiming to expand applicability in industrial and service robotics.

#### REFERENCES

Ansari, U., Pramod, A. S., Varala, N., & Asokan, T. (2025, July). Design and analysis of a multi-chamber, multi-curvature soft pneumatic actuator for controlled directional bending actuation. In AIR 2025 (to appear).

Ariyanto, M., Mulyanto, D., Munadi, M., Nugroho, T., & Setiawan, J. D. (2019). Three-fingered soft robotic gripper based on pneumatic network actuator. In 2019 6th International Conference on Information Technology, Computer, and Electrical Engineering (ICITACEE) (pp. 1–6). IEEE.

Benyus, J. M. (1997). Biomimicry: Innovation inspired by nature. Harper Perennial.

Calisti, M., Giorelli, M., Levy, G., Mazzolai, B., Hochner, B., Laschi, C., & Dario, P. (2011). An octopusbioinspired solution to movement and manipulation for soft robots. Bioinspiration & Biomimetics, 6(3), 036002.

Dassault Systèmes. (2021). Abaqus/CAE User's Guide (Version 2021). Dassault Systèmes Simulia Corp.

Gariya, N., Asrani, A., Kumar, S., & Nautiyal, H. (2023). Bending mechanics of the soft pneumatic single air chamber bending actuator.

Gariya, N., Kumar, P., Prasad, B., & Singh, T. (2023). Soft pneumatic actuator with an embedded flexible polymeric piezoelectric membrane for sensing bending deformation. Materials Today Communications, 35, 105910.

Hu, W., Mutlu, R., Li, W., & Alici, G. (2018). A structural optimisation method for a soft pneumatic actuator. Robotics, 7(2), 24.

Huang, W., Xiao, J., & Xu, Z. (2021). A variable structure pneumatic soft robot. *Scientific Reports*, 11, 1–10.

Lei, J., Ge, Z., Fan, P., Zou, W., Jiang, T., & Dong, L. (2022). Design and Manufacture of a Flexible Pneumatic Soft Gripper. *Applied Sciences*, 12(13), 6306.

- Mosadegh, B., Polygerinos, P., Keplinger, C., Wennstedt, S., Shepherd, R. F., Gupta, U., Shim, J., Bertoldi, K., Walsh, C. J., & Whitesides, G. M. (2014). Pneumatic networks for soft robotics that actuate rapidly. Advanced Functional Materials, 24(15), 2163–2170
- Navas, E., Fernandez, R., Sepúlveda, D., Armada, M., & Gonzalez-de Santos, P. (2021). Soft grippers for automatic crop harvesting: A review. Sensors, 21(8), 2689.
- Ogden, R. W. (1997). *Nonlinear elastic deformations* (2nd ed.). Dover Publications.
- Polygerinos, P., Wang, Z., Overvelde, J. T. B., Galloway, K. C., Wood, R. J., Bertoldi, K., & Walsh, C. J. (2015). Modeling of soft fiber-reinforced bending actuators. *IEEE Transactions on Robotics*, 31(3), 778–789.
- Qin, L., Peng, H., Huang, X., Liu, M., & Huang, W. (2023). Modeling and simulation of dynamics in soft robotics: A review of numerical approaches. *Current Robotics Reports*, 5(1), 1–13.
- Rogóż, M., Zeng, H., Xuan, C., Wiersma, D. S., & Wasylczyk, P. (2016). Soft robotics: Light-driven soft robot mimics caterpillar locomotion in natural scale. Advanced Optical Materials, 4(11), 1902–1906.
- Singh, K. S., & Asokan, T. (2019, October). Design and analysis of a soft bidirectional bending actuator for human-robot interaction applications. In 2019 28th IEEE International Conference on Robot and Human Interactive Communication (RO-MAN) (pp. 1–6). IEEE.
- Song, E. J., Lee, J. S., Moon, H., Choi, H. R., & Koo, J. C. (2021). A multi-curvature, variable stiffness soft gripper for enhanced grasping operations. Actuators, 10(12), 316.
- Su, H., Hou, X., Zhang, X., Qi, W., Cai, S., Xiong, X., & Guo, J. (2022). Pneumatic soft robots: Challenges and benefits. *Actuators*, 11(3), 92.
- Sun, Y., Zhang, Q., Chen, X., & Chen, H. (2019). An optimum design method of Pneu-Net actuators for trajectory matching utilizing a bending model and GA. *Journal of Robotics*, 2019, 6721897.
- Tang, X., Li, H., Ma, T., Yang, Y., Luo, J., Wang, H., & Jiang, P. (2022). A review of soft actuator motion: Actuation, design, manufacturing and applications. Actuators, 11(11), 331.
- Wu, Y., Yim, J. K., Liang, J., Shao, Z., Qi, M., Zhong, J., & Lin, L. (2019). Insect-scale fast-moving and ultrarobust soft robot. Science Robotics, 4(32), eaax1594.
- Yang, F., Ruan, Q., Man, Y., Xie, Z., Yue, H., Li, B., & Liu, R. (2020). Design and optimize of a novel segmented soft pneumatic actuator. *IEEE Access*, 8, 3006865– 3006877.
- Yeoh, O. H. (1993). Some forms of the strain energy function for rubber. *Rubber Chemistry and Technology*, 66(5), 754–771.
- Zhang, H., Kumar, S., Chen, F., Fuh, J. Y. H., & Wang, M. Y. (2019). Topology optimized multimaterial soft fingers for applications on grippers, rehabilitation, and artificial hands. *IEEE/ASME Transactions on Mechatronics*, 24(1), 120–131.

- Zhang, J., Wang, T., & Hong, J. (2017). Review of soft-bodied manipulator. *Journal of Mechanical Engineering*, 53(13), 19–28.
- Zaidi, S., Maselli, M., Laschi, C., & Cianchetti, M. (2021). Actuation technologies for soft robot grippers and manipulators: A review. *Current Robotics Reports*, 2(3), 167–181.

